AJNR Am J Neuroradiol 26:1612–1622, August 2005

Evaluation of the Pathologic Characteristics of Excitotoxic Spinal Cord Injury with MR Imaging

Sara A. Berens, Daniel C. Colvin, Chen-Guang Yu, Robert P. Yezierski, and Thomas H. Mareci

BACKGROUND AND PURPOSE: **Although high-resolution MR imaging is a valuable diagnostic tool, in vivo MR imaging has not yet been compared with in vitro MR imaging and histologic techniques following experimental spinal cord injury (SCI). The goal of the present study was to evaluate the feasibility of using in vivo MR imaging, in vitro MR imaging, and histologic techniques to study pathologic changes associated with excitotoxic SCI at a single time point. These results are important for future research using in vivo MR imaging to study the temporal profile of pathologic changes following SCI.**

METHODS: **Rats received intraspinal injections of quisqualic acid at the T12–L2 spinal level. In vivo T1- and T2-weighted and dynamic contrast-enhanced MR images were collected 17–24 days postinjury. Once completed, spinal cords were removed and in vitro MR microscopy and histologic assessment were performed. MR images were collected using 4.7-T (in vivo) and 14.1-T magnets (in vitro).**

RESULTS: **Pathologic changes—including hemorrhage, neuronal loss, cavities, and central canal expansion—were visible in T2-weighted in vivo MR images. Evaluation of the blood–spinal cord barrier after injury with contrast agent enhancement showed no disruption at the time points evaluated. In vitro MR images and histologic evaluation confirmed pathologic details observed in vivo.**

CONCLUSION: **Results show that high-resolution in vivo MR imaging has the potential to be used in studying the progression of pathologic changes at multiple time points following SCI. This strategy may provide a way of studying structure-function relationships between therapeutic interventions and different pathologic characteristics of the injured spinal cord.**

The intraspinal injection of the alpha-amino-3-hydroxl-5-methyl-4-isoxazole-propionate/metabotrophic receptor agonist, quisqualic acid (QUIS), produces an excitotoxic spinal cord injury (SCI), which has been used to study the molecular, pathophysiologic, and behavioral characteristics of SCI (1). These injections result in pathologic changes similar to those associated with ischemic and traumatic SCI (2, 3). Although most of what is known about the pathologic changes associated with experimental SCI (ie, edema, neuronal loss, hemorrhage, and cavitation) has come from histologic studies, noninvasive high-resolution MR imaging is becoming a preferred method for the visualization of SCI (4–6). In recent years, MR imaging has become a valuable diagnostic tool in studies examining the pathologic changes following SCI (7–14). One well-documented change associated with SCI is the breakdown of the blood–spinal cord barrier (BSCB). The pathologic characteristics associated with BSCB disruption following SCI can be measured quantitatively with dynamic contrast-enhanced MR imaging (DCE-MR imaging), by using exogenous paramagnetic contrast agents (15–18). Fine details of SCI pathology can also be determined with intact excised cords by using MR microscopy. With this technique, motion artifacts are eliminated, allowing the signal intensity–to-noise ratio (SNR) to be optimized with prolonged scan times and higher field strengths (19).

Received October 11, 2004; accepted after revision December 6.

From the Comprehensive Center for Pain Research (S.A.B., C.-G.Y., R.P.Y.), Center for Structural Biology (T.H.M.), and McKnight Brain Institute (S.A.B., R.P.Y., T.H.M.) and the Departments of Biochemistry and Molecular Biology (T.H.M.), Neuroscience (R.P.Y.), and Physics (D.C.C., T.H.M.), University of Florida, Gainesville, FL.

A preliminary description of this study was reported in an abstract at the National Neurotrauma Society Symposium 2003: Berens SA, Yezierski RP, Mareci TH. Application of *in vivo* magnetic resonance imaging to define the pathological characteristics of excitotoxic spinal cord injury. National Neurotrauma Society Symposium, November 2003, Biloxi, MS.

Address correspondence to Thomas H. Mareci, PhD, Department of Biochemistry and Molecular Biology, University of Florida, 100 Newell Drive, Room LG-183, P.O. Box 100245, Gainesville, FL 32610-0245.

Thus far, the pathologic characteristics determined with in vivo MR imaging have not been compared with in vitro MR imaging and histologic examination by using the excitotoxic injury model. We hypothesize that in vivo MR imaging has the sensitivity to detect significant differences in pathologic characteristics between two different strategies of injury, which can be correlated with in vitro MR imaging and histology.

Methods

All experiments were carried out in accordance with National Institutes of Health guidelines for the care and use of animals and approved by the University of Florida Institutional Animal Care and Use Committee. In vivo and in vitro MR methods, along with histologic techniques, were used, because these were the most direct measures of pathologic changes following injury. A comparison of findings with different methods was carried out. Future studies will use diffusion-weighted MR imaging and fiber mapping.

Animal Preparation

The technique of intraspinal injection was similar to that described elsewhere (3). In brief, Sprague-Dawley male rats weighing 250–300 g were anesthetized with a mixture of ketamine (3.0 mL), acepromazine (1.0 mL), and xylazine (3.0 mL; mixture at 0.65 mL/kg, subcutaneously). Supplemental doses of anesthetic were given, if necessary, when rats responded to a noxious pinch applied to the glabrous skin of an extended hind paw. Animals were placed in a stereotaxic frame and the vertebral column immobilized with a vertebral clamp. One injection window for intraspinal injections was made by laminectomy between spinal segments T12–L2. Once the cord was exposed, the dura was incised longitudinally and reflected bilaterally. A small hole for unilateral injections was made in the pia mater. After injection, muscles were closed in layers and the skin was closed with wound clips. The day following the final in vivo image acquisition, animals were anesthetized with sodium pentobarbital and euthanized by transcardial perfusion with normal saline followed by 10% formalin. Spinal cords were removed and stored in 10% formalin.

Intraspinal Injection Procedure

Before injection, QUIS, 125 mmol/L, was mixed in sterile saline, corrected to physiologic pH, and was then injected unilaterally at one level of the cord (T12–L2). To compare injury pathology between lesions at different depths, two types of injection strategies were used: injections at a depth of 500 μm (QUIS lesion 1 [QL1], two animals) and at a depth of 1000 μm (QUIS lesion 2 [QL2], five animals) below the surface (20). Injections were made between the dorsal root entry zone and the dorsal vein on the right or left side, depending on vascularity on the surface of the cord. The total volume of QUIS injected was 1.2 μL in three tracks (0.4 μL/track; distance between tracks 0.5 mm in the rostrocaudal direction). A Hamilton microliter syringe with a glass micropipette extension (tip diameter, 5–10 μm) was used for intraspinal injections. The syringe was positioned in a microinjector unit (Kopf 5000; Kopf, Tujunga, CA) attached to a micromanipulator. A sham injury group was prepared by injecting saline in the same manner as described above.

In Vivo MR Imaging

On the basis of previous correlations between the extent of pathology and the temporal onset of injury-induced behavioral changes, in vivo MR imaging was performed 17–24 days (mean, 22 days) after injury (21, 22). Animals were initially anesthetized by inhalation of a mixture of 5% isofluorane with oxygen at a flow rate of 2 L/min and maintained via a nose cone with a mixture of 2% isofluorane with oxygen at a flow rate of 1 L/min. To determine whether there was disruption of the BSCB following injury, DCE-MR imaging was performed with the intravenous injection of gadolinium-diethylene-triamine-pentaacetic, bis-methylamine ([Gd] Omniscan, Nycomed, Oslo). For intravenous delivery of Gd, the tail vein was canulated with a 24-G, .75-inch intravenous catheter (Terumo Surflo, Webster Veterinary Supply, Inc., Sterling, MA). Before catheterization, the catheter was filled with heparin solution (mixture of 6 mL of saline and 0.2 mL of 1000 U/mL) to prevent clotting. Once the catheter was in place, a syringe filled with the appropriate volume (0.6 mL/kg body weight) of Gd (0.3 mmol/kg) was attached to the catheter and stabilized with surgical tape. A pulse oximeter was used on the tail to monitor heart rate and blood oxygenation saturation. Core body temperature was monitored during experiments by using a rectal probe and was kept between 35°C and 37°C. Respiration rate was also monitored during data acquisition.

In Vivo High-Resolution MR Imaging Data Acquisition

All in vivo NMR measurements were performed on a 4.7T, 33-cm-bore Oxford magnet (Oxford Instruments, Oxford, UK) at 200 MHz by using a Bruker BIOSPEC Avance DBX console (Bruker NMR Instruments, Billeria, MA) and 100 mT/m actively shielded gradients. A highly sensitive quadrature MR surface coil was constructed specifically for imaging the rat spinal cord. The coil consisted of two rectangular overlapping coil elements (3 × 3 cm), constructed by using copper tape, placed on the inside of a half-cylinder cradle 4 cm in diameter. All data acquisition was performed with Bruker ParaVision software. General image processing and analysis of the time series DCE data were performed by using custom software written in the Interactive Data Language (Research Systems, Boulder, CO).

Rats were placed supine in a custom-built half cylinder cradle/coil apparatus. The 200-MHz quadrature MR surface coil was tuned with a Hewlett Packard HP8752C network analyzer (Hewlett Packard, Englewood, CO). The position of the animal was confirmed with pilot images to locate the injury site. Pilot images were T1 weighted (TR/TE = 500 ms/5 ms; NA = 1), with a field of view (FOV) of 6 cm in each direction, a 1 mm section, and a 128 × 128 matrix. Fat suppression was done by using a CHESS-type sequence (23). Once the position was confirmed, a set of fat-suppressed, high-resolution sagittal and transverse images was collected. Sagittal T1-weighted (TR/TE = 1000 ms/10.5 ms; NA = 4) spin-echo images were acquired over five sections, each 1 mm thick without a gap between sections. A TR of 1000 ms was chosen to provide optimum signal intensity strength with T1-weighting for anatomic definition. Additional acquisition parameters were a FOV of 4 cm × 2 cm, read out in the head-to-foot direction, and a matrix of 256 × 128. The scan time with these parameters was 8.67 minutes. Transverse T1-weighted (TR/TE = 1000 ms/10.5 ms; NA = 4) spin-echo images were acquired over 14 sections, each 1 mm thick without a gap between sections. Other acquisition parameters were a FOV of 2 cm × 2 cm, read out in the anteroposterior direction, and a matrix of 128 × 128. The scan time was 8.67 minutes.

Sagittal T2-weighted (TR/effective TE = 2000 ms/62.5 ms; NA = 6) fast spin-echo images with phase-encode segmentation were acquired over five sections, each 1 mm thick without a gap between sections. Additional acquisition parameters were a FOV of 4 cm × 2 cm, read out in the head-to-foot direction, phase-encode segmentation factor of 4, and a matrix of 256 × 128. The scan time with these parameters was 6.5 minutes. Transverse T2-weighted (TR/effective TE = 2000 ms/62.5 ms, NA = 6) fast spin-echo images with phase-encode segmentation were acquired over 14 sections, each 1 mm thick

without a gap between sections. Other acquisition parameters were a FOV of 2 cm × 2 cm, read out in the anteroposterior direction, phase-encode segmentation factor of 4, and a matrix of 128 × 128. The scan time with these parameters was 6.5 minutes.

In Vivo DCE-MR Imaging Data Acquisition

After four sets of high-resolution images were collected, a series of dynamic contrast-enhanced images of the rat spinal cord was acquired. Transverse and sagittal images were acquired before and after the contrast agent was injected. Transverse images were acquired with a FOV of 2 cm × 2 cm and a matrix of 64 × 64, over eight sections, and sagittal images with a FOV of 4 cm × 2 cm and a matrix of 128 × 64, over three sections, both 1 mm thick without a gap between sections. Three sets (transverse and sagittal interleaved) of T1-weighted precontrast multisection images (TR/TE = 330 ms/9.4 ms; NA = 8) were collected. After acquisition of the precontrast images, Gd was injected in approximately 5 seconds with continuous pressure, to prevent backflow, through the implanted catheter while the animal was in the magnet. Immediately after injection, 8–10 sets (6 minutes for each set) of T1-weighted postcontrast multisection images (TR/TE = 330 ms/9.4 ms; NA = 8) were collected, with transverse and sagittal data-set acquisitions interleaved. We collected these images over a 60-minute time frame, which was chosen on the basis of previous experience, with a peak enhancement for the cord at 3 minutes. The receiver gain was adjusted to one-third the value used for the high-resolution images because Gd provides approximately three times the contrast enhancement.

In Vitro MR Microscopy

All in vitro NMR measurements were performed on a 14.1T, 51-mm-bore Oxford magnet, at 600 MHz, by using a Bruker BIOSPEC Avance DBX console. All data acquisition was performed with Bruker ParaVision software. Before imaging, spinal cords were placed in phosphate-buffered saline (PBS) overnight. The cords were placed in 5-mm tubes and imaged in PBS by using a standard 5-mm MR coil. Three sets of high-resolution multislice two-dimensional images oriented in three orthogonal directions were collected (TR/TE = 2500 ms/20 ms; NA = 8). The transverse images were acquired over 60 sections (200 μm thick without a gap between sections; FOV = 5 mm × 5 mm; matrix = 256 × 256), the sagittal images were acquired over 20 sections (200 μm thick without a gap between sections; FOV = 20 mm × 5 mm; matrix = 1024 × 256), and the coronal images were acquired over 20 sections (200 μm thick without a gap between sections; FOV = 20 mm × 5 mm; matrix = 1024 × 256). Immediately after the final imaging session, spinal cords were placed in fixative. General image processing and analysis was performed by using custom software written in the Interactive Data Language (IDL, from Research Systems, Boulder, CO).

Histologic Procedures

Once imaging was completed, spinal cords were placed in 10% sucrose overnight. Serial sections (75 μm) were cut on a freezing microtome, collected in PBS, and mounted on gelatin-coated slides. Sections were stained with cresyl violet and cover-slipped. To confirm that the hypointense signals from MR images correlated with hemorrhage, sections sampled from the injury site were stained with the Prussian-blue reaction (24).

Data Analysis

To compare results obtained with the three different methods used, total longitudinal injury lengths were determined. Statistical analysis of these data included a repeated-measures ANOVA test to determine differences in distances determined by the three methods (SPSS, Chicago, IL). This was followed by a paired comparison to interpret the significance of the ANOVA. To determine the total longitudinal injury length, the total number of transverse sections from each method, with evidence of excitotoxic (ie, cavity formation, hemorrhage, and neuronal loss) damage (3, 21, 25), were counted and multiplied by the section thickness appropriate for the method used. Transverse images were used for injury length calculation instead of sagittal images, because the boundaries of the injury (eg, neuronal loss in the dorsal horn—a classical characteristic of excitotoxic SCI) were best observed in transverse images. For the calculation of injury length by using in vivo MR imaging, T2-weighted transverse images were counted and multiplied by 1 mm; for in vitro MR imaging, transverse images were counted and multiplied by 200 μm; and for histology, sections were counted and multiplied by 75 μm (21). Histologic determination of injury length was done via microscopic examination with 4× and 10× objectives. In addition to injury length, pathologic characteristics (ie, cavity formation, central canal expansion, hemorrhage, and neuronal loss) of the injury were compared between the two types of injection strategies used (ie, QL1 vs QL2).

For DCE-MR imaging processing, regions of interest (region of interest) were selected in the injured and normal cord, muscle, and bone. A 1-mm × 2-mm elliptical region of interest was drawn in regions of injury and normal cord because the enhanced region was typically elliptical. A 1-mm circle region of interest was drawn for muscle and bone and was analyzed to determine the success of the Gd injection. Ten percent peak enhancement was used as the cutoff value because regions of interest of normal cord showed 10% peak enhancement because of the presence of contrast agent in the cord vasculature.

Results

In Vivo High-Resolution MR Imaging

Figure 1 shows a comparison of the pathologic findings from the same animal (S05) at the same location for all three methods used in this study. The appearance of images was compared with normal controls. When an image region relative to a control region appeared darker, we classified it as hypointense. When an image region relative to a control region appeared brighter, we classified it as hyperintense. No signal intensity changes were observed in the normal cord on either T1-weighted (T1-weighted) or T2-weighted (T2-weighted) images (data not shown). The only significant information obtained from T1-weighted images of QUIS-injured animals was the injection tracks, which were seen as weak hypointense (ie, dark) signals.

Figures 2*A* and 3*A* show the sagittal and transverse T2-weighted in vivo images, respectively, for each injured animal. Using in vivo transverse images, it was possible to determine the anatomic level of the sections by examining the size and shape of the cord as well as gray and white matter. Injection tracts for QUIS injections were visible in both T2-weighted (Figs 1 and 3) and T1-weighted transverse images (not shown) in all animals. Hypointense (ie, dark) signals can be seen within the cord on T2-weighted images of all QUIS-injured animals; however only T2-weighted in vivo images of QL2 animals (S01, S02, and S04–S06) showed hyperintense (ie, bright) signals.

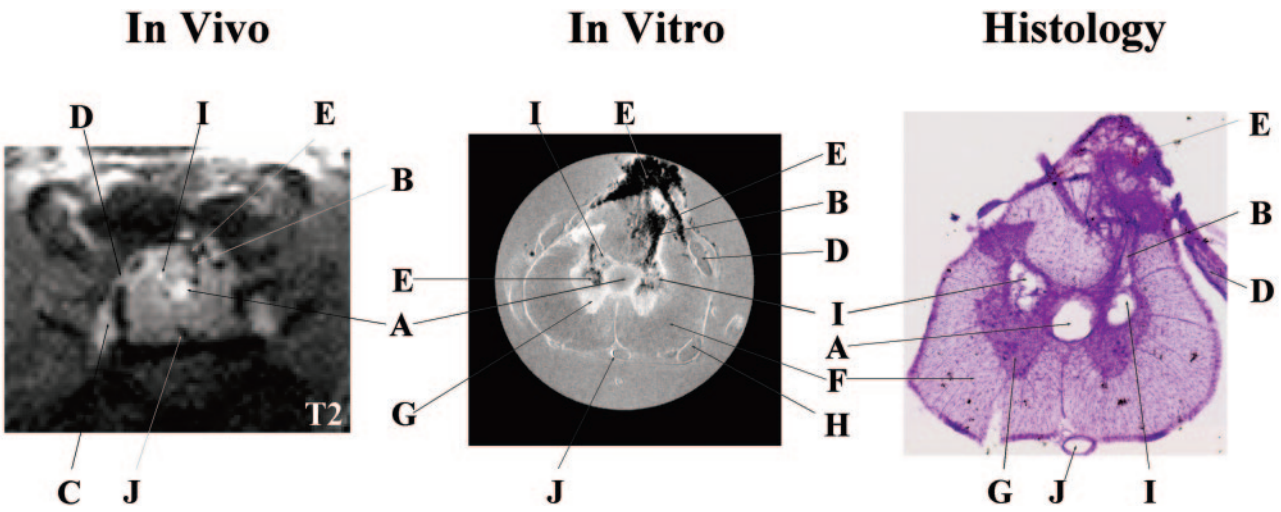

FIG 1. Representative pathologic findings in the same animal (S05) at the same location observed in vivo (T2-weighted, TR/effective − TE = 2000 ms/62.5 ms; NA = 6), in vitro (TR/TE = 2500 ms/20 ms; NA = 8), and in histologic sections. Many of the same pathologic details are visible with all three methods albeit with different levels of resolution. In vivo and in vitro images are displayed with image size = 0.92 cm × 0.77 cm (in vivo) and 0.50 cm × 0.50 cm (in vitro). Letters label the most distinctive anatomic and pathologic characteristics observed in the three images as follows: A indicates expanded central canal; B, injection track; C, dorsal root ganglion; D, dorsal root; E, hemorrhage at injury site; F, white matter; G, gray matter; H, ventral root; I, cavity; J, anterior spinal vessel. In vivo images show cavitation as hyperintense signals due to T2 weighting, whereas, on in vitro images, cavities appear isointense in these proton attenuation-weighted images.

In vivo images showed consistent differences between QL1 and QL2 animals (Figs 4–6). It is important to note that hyperintense signals, indicating expansion of the central canal and cavitation, were not seen in images from QL1 animals (Fig 3*A;* X01 and X03; Fig 6). Although the only difference in QUIS injection parameters was depth of injection, there were dramatic differences in the extent of pathologic damage (eg, laterality, cavitation, and expansion of the central canal). There were also distinctive differences in injury lengths between QL1 (X01 and X03) and QL2 animals (S01, S02, and S04–S06; Fig 4).

In Vivo DCE-MR Imaging

To determine whether there was BSCB disruption at the 17–24-day interval (mean = 22 days) postinjury, DCE-MR imaging was performed by using Gd as a contrast agent. Disruption of the BSCB was indicated by a significant Gd enhancement (>10%) within the cord at the site of injury. No significant Gd enhancement was observed in the normal and sham groups and no significant Gd enhancement was observed within the cord at the site of injury in any of the QUIS-injured animals. Gd enhancement, however, was observed in surrounding muscle of all animals, approximately 300% peak signal intensity enhancement, which indicates that the procedure was performed correctly.

In Vitro MR Microscopy

Images obtained in vitro had greater resolution and more clearly defined the pathologic characteristics (ie, neuronal loss, hemorrhage, and cavitation) of the injury compared with the in vivo MR images. No abnormal signals were observed in the normal control animal. For the saline-injected animal, however, a hypointense (ie, dark) region was observed at the site of injection, which correlated with hemorrhage (see "Histologic Findings"). Figures 2*B* and 3*B* illustrate the sagittal and transverse in vitro images, respectively, at the epicenter for each QUIS-injured animal. In both sagittal and transverse images, white matter and gray matter were clearly distinguishable and the cord level was easily determined. In all QUIS-injured animals, hypointense regions were observed at the site of injury, correlating with hemorrhage.

Total injury lengths measured with in vitro MR images were significantly greater than lengths determined with in vivo MR images, because of differences in section thickness (Fig 4); repeated-measures ANOVA ($F = 40.476$; $P = .001$). Pair-wise comparisons indicated that in vivo MR imaging gave significantly shorter injury lengths than in vitro MR imaging ($P < .001$) and histology ($P < .001$), but were within the range of difference in section thickness (length difference standard deviation = 0.50 mm) for each method used (section thickness in vitro of 0.2 mm and in vivo of 1.0 mm).

Histologic Findings

Histologic results confirmed the pathologic characteristics observed with in vivo and in vitro MR imaging. Injection tracts were visible in all QUIS-injured animals, as well as saline-injected animals. Neuronal loss in the dorsal horn ipsilateral to the injury was observed in all QUIS-injured animals. Neuronal loss in the dorsal horn contralateral to the injection site was observed in all QL2 animals but not in QL1 animals. Central canal expansion was observed in four of five QL2 animals and cavity formation was observed only in QL2 animals, being present both

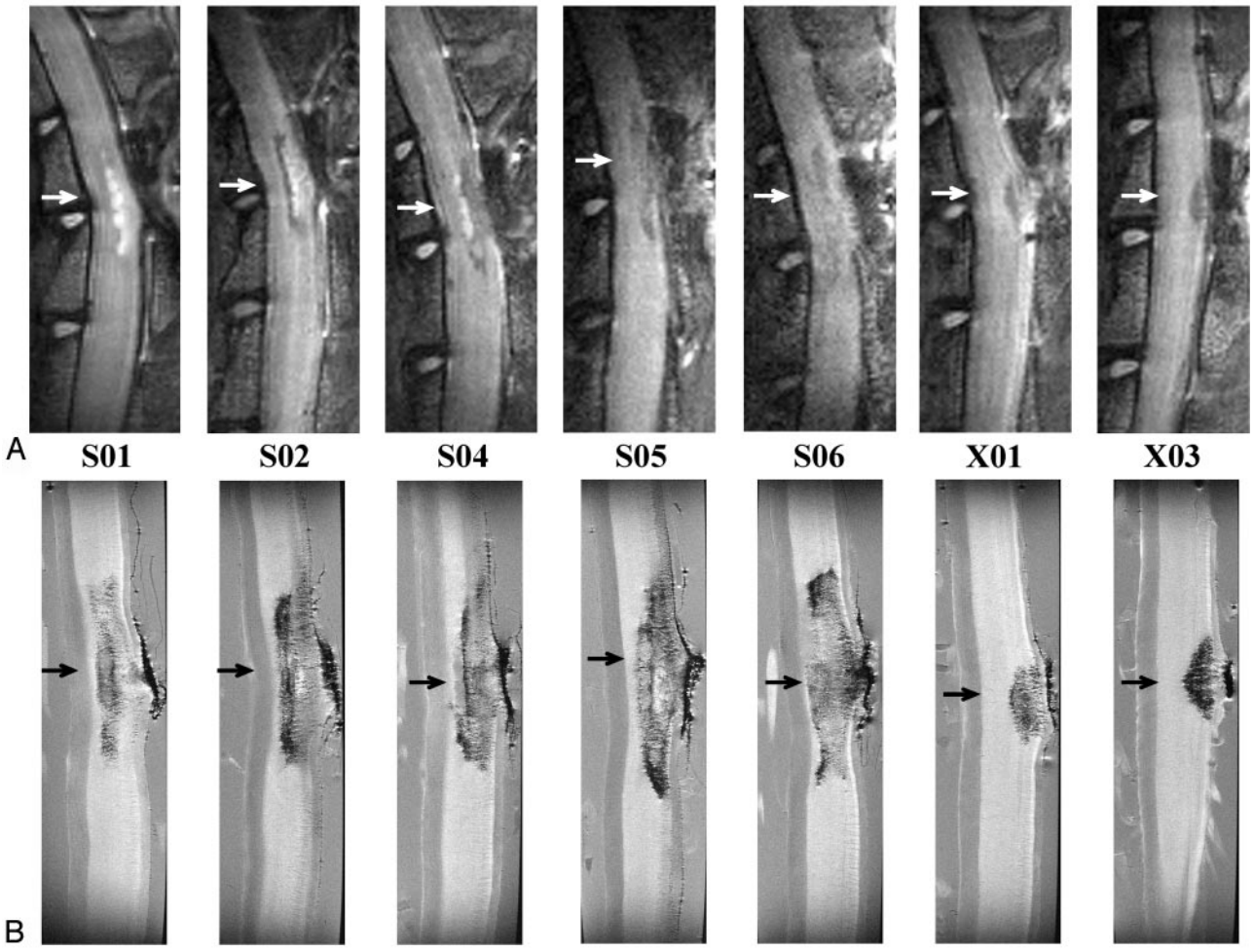

FIG 2. *A,* In vivo (T2-weighted, TR/effective TE = 2000 ms/62.5 ms; NA = 6); and, *B,* in vitro (TR/TE = 2500 ms/20 ms; NA = 8) sagittal images for all QUIS-injured animals. Images are oriented with rostral at the top and dorsal on the right. *Arrows* represent the location of the epicenter of the injury. The epicenter was defined as the region of maximal pathologic damage. Displayed image size = 0.77 cm × 2.15 cm (in vivo) and 0.40 cm × 1.50 cm (in vitro). Animals designated S01, S02, S04, S05, and S06 received QL2, whereas animals designated X01 and X03 received QL1. The vertebral column and laminectomy site were easily observed in both in vivo and in vitro sagittal images.

ipsilateral and contralateral to the side of QUIS injection. Sections from three of three animals (S01, S06, and X03) stained positive for the Prussian Blue reaction, confirming the presence of hemorrhage at the same location of hypointense signal intensity as observed in the in vivo and in vitro images.

Because of histologic artifacts, complete injury lengths could not be determined for all cords. In animals with minimal histologic damage (all but X03), however, the total injury lengths determined from histologic evaluation showed no significant differences to those determined with in vitro images (Fig 4; $P > .05$).

Figures 5 and 6 show a summary of data collected from a representative QL2 (S06) and QL1 (X03) animal, respectively. Sufficient detail is visible in the in vivo images to determine the type and extent of pathologic damage. There was narrowing of the dorsal horn with sparing of the superficial laminae bilaterally in all QL2 animals. This is in contrast to QL1 animals, in which sparing was observed only unilaterally. A significant observation in this study was that following the more superficial injury (laminae I–III, QL1); damage occurred only ipsilateral to the side of QUIS injections and included only evidence of hemorrhage. In contrast, lesions deeper in the gray matter (QL2) produced damage both ipsilateral and contralateral to the injection site, showing evidence of both hemorrhage and cavitation. In addition, evidence for differences between QL1 and QL2 injuries were seen in the rostrocaudal and ventral extent of injury (eg, less extensive in QL1 animals compared with QL2 animals [Fig 6]).

Discussion

Clinically, MR imaging has been a useful tool for the study of secondary complications associated with SCI. For example, MR imaging can play an important role in the study of post-traumatic syringomyelia. The excitotoxic injury model has been shown to produce pathologic changes similar to those observed in this condition (2, 26). Considering the lack of understanding of the pathologic mechanism responsible for cav-

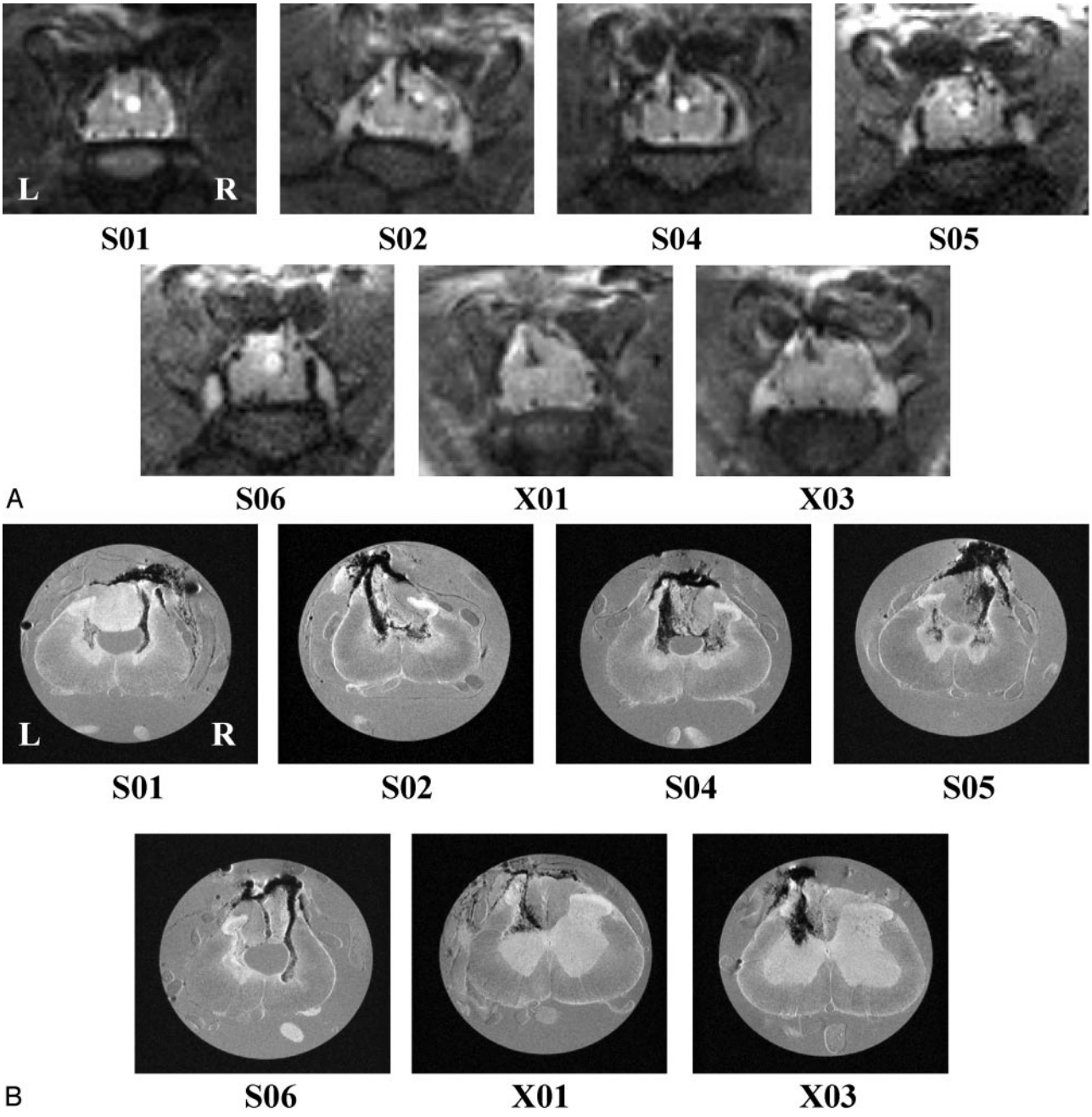

FIG 3. *A,* In vivo (T2-weighted, TR/effective − TE = 2000 ms/62.5 ms; NA = 6); and, *B,* in vitro (TR/TE = 2500 ms/20 ms; NA = 8) transverse images for all QUIS-injured animals. Images are sampled from the epicenter of the injury (*arrows* in Fig 2) and show comparable pathologic changes between methods. See Fig 1 for labeling of anatomic and pathologic findings. Images are oriented with dorsal at the top. *L,* left side of cord; *R,* right side of cord, for all images. Displayed image size = 0.92 cm × 0.77 cm (in vivo) and 0.50 cm × 0.50 cm (in vitro). *A,* Hypointense signals correlated with hemorrhage (see "Histologic Findings") and hyperintense signals correlated with the presence of fluid filled cavities. For example, notice the hyperintense expanded central canal in the cord of animals S01, S02, and S04–S06 and the hyperintense cavity in the gray matter on the right side of the cord in animal S02. *B,* Hypointense regions were observed bilaterally in the gray matter in all QL2 animals (S01, S02, and S04–S06), whereas, in QL1 animals, evidence of hemorrhage was observed only ipsilateral to the side of QUIS injection (X01 and X03). In addition, hypointense areas were observed in the dorsal columns in all the QUIS-injured animals except S01. Central canal expansion was clearly defined in four of the five QL2 animals (S01 and S04–S06), and injection tracks were visible in all injured animals. Cavity formation was also seen in all QL2 animals bilaterally.

ity formation in the injured cord (27), it may be possible to gain insight into the mechanism of cavitation by using in vivo MR imaging at different time points following excitotoxic SCI. In the past, clinicians have relied on patient descriptions of behavioral changes in determining clinical outcome (28, 29); however, MR imaging recently has been used to monitor changes associated with intraspinal transplantation, graft-mediated functional recovery, and changes in syrinx morphology after transplantation (30) and to

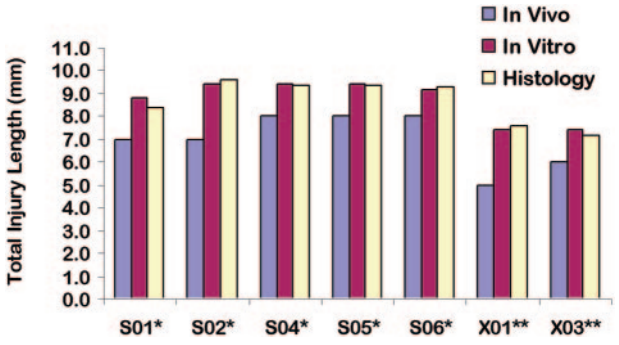

FIG 4. Total injury lengths determined by using in vivo, in vitro, and histologic methods for each QUIS-injured animal. Total injury lengths in millimeters reflect the presence of excitotoxic tissue damage. No significant differences are observed between in vitro and histology ($P > .05$). Significant differences are observed between in vivo and in vitro/histology ($P < .05$), but these differences are within the range of section thickness difference between in vivo and in vitro images. A single asterisk denotes the QL2 animal, and double asterisks denote the QL1 animal.

differentiate between cyst and scar or tumor formation with the help of MR contrast agent administration (26). With the importance and many uses for MR imaging, continued research is needed to enhance this technique and expand its uses to provide a better understanding of the mechanisms responsible for pathologic changes associated with SCI. For example, an important question related to SCI is the temporal profile of pathologic changes in the acute and chronic stages postinjury. Using in vivo MR imaging, it should be possible to monitor these changes in the same animal. In the present study the feasibility of using a complement of in vivo and in vitro MR imaging, along with histologic methods to study experimental SCI was examined.

The results have shown that MR images provide details of pathologic changes, which correlated with histologic findings, and were easily detected both in vivo and in vitro. These changes include cavities, central canal expansion, hemorrhage, and tissue loss. These characteristics of injury are similar to those previously reported in both experimental (4, 5, 6, 31–35) and clinical studies (7–14, 31). The present study is one of the first that has attempted to compare all three methods (see also a recent study in the mouse by Bonny et al [36]).

An important finding in this study was the sensitivity of in vivo MR imaging to detect differences in pathology between two different strategies of injury. Despite the small differences in injury depths between QL1 and QL2, there were significant differences in the overall pathology detected in the in vivo MR images. Following the shallower injury (ie, QL1), damage was observed only unilaterally in the gray matter and did not show any cavitation or central canal expansion. In contrast, following the deeper injury (ie, QL2), damage was more severe, and showed cavitation, hemorrhage, and neuronal loss bilaterally. These differences could be due to the connectivity between regions of the cord at different depths in the gray matter. For example, propriospinal connections involving laminae IV–VII are far more extensive within and between segments than those involving more superficial laminae (37, 38). Although speculative, it is possible that, once damaged, a signal intensity is relayed to other parts of the gray matter that induces further damage. The deeper lesion (QL2) resulted in damage of the contralateral side of the cord similar in pathologic characteristics to the side that received the QUIS injection. This suggests a similar mechanism of injury (ie, excitotoxicity). From this, one might conclude that propriospinal connections exert a trophic influence on other parts of the gray matter and once damaged, leads to an injury induced release of excitatory amino acids and subsequent pathologic changes. This observation may be important from the standpoint of providing insight into the mechanism responsible for the progression of pathologic changes following spinal injury.

There was a corresponding loss of gray matter illustrated in in vitro MR images and histology. These changes could be quantified with sufficient information about volumes of normal white and gray matter. Although volume quantification of white and gray matter loss is important, it was beyond the scope of this study. It will, however, be considered in future studies.

All three methods used in this study were directly compared, because they all showed similar pathologic changes. For example, in vitro MR images were the most precise in determining injury length, rather than histologic sections due to histologic artifacts. Although significant differences were detected between total lengths of injury, these differences were within the thickness of sections of the methods used. For this reason, the present data support the conclusion that in vivo MR imaging is a useful technique to study the evolution of pathologic changes following SCI. This feature may be especially important when correlated with the profile of changes related to the disruption of the BSCB.

The observation of changes in the BSCB is important in characterizing the excitotoxic model of SCI, because BSCB disruption can contribute to events leading to detrimental pathologic processes following SCI (39, 40). At the time points used in this study, 17–24 days postinjury, our measurement of the BSCB indicated that the barrier was intact; however, previous studies indicate an opening at earlier time points following contusion injury (15, 16). Therefore, longitudinal studies will be necessary to detect the temporal characteristics of how the BSCB is affected following excitotoxic SCI. Preliminary data from an ongoing study suggest that there are changes over time in the integrity of the BSCB following excitotoxic injury (S. A. Berens, P. Yezierski, T. H. Mareci, unpublished observations).

There are several advantages and disadvantages associated with each of the methods used in the present study. In vivo MR imaging can be used to noninvasively monitor the progression of pathologic changes over time in the same animal. This feature provides the opportunity to study the neuroprotective

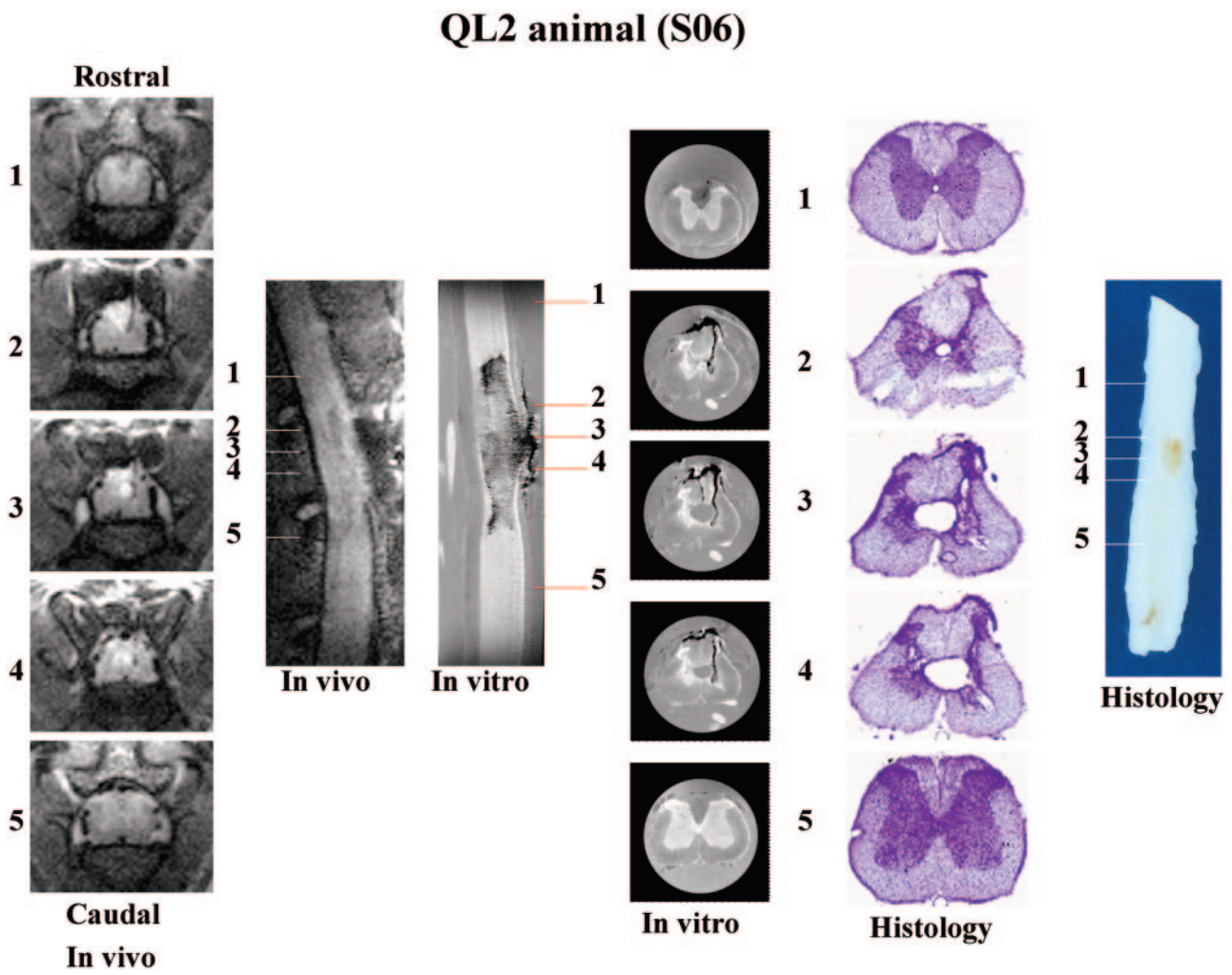

FIG 5. Summary of in vivo, in vitro, and histologic data collected for a representative QL2 animal (S06). Representative sections (1–5) are sampled from the same rostrocaudal location in the spinal cord with each method used. Image sizes are the same as in Figs 2 and 3. See Fig 1, for labeling of anatomic and pathologic findings. Although sagittal images show the rostral-caudal extent of the injury, transverse sections provide greater detail of the pathologic changes associated with this injury model.

and neurorestorative properties of therapeutic interventions (eg, transplants, drugs, etc). In vivo MR imaging methods, however, lack the higher resolution that in vitro MR imaging and histologic methods provide. Despite the higher resolution, in vitro MR imaging and histologic methods have the disadvantage that they cannot be used at different time points in the same animal, and there is a risk of losing tissue in histologic analysis because of processing artifacts. Another advantage of in vivo MR imaging is the ability to analyze the injured cord in transverse and sagittal planes of section at different time points in the same animal. This capability allows one to easily determine the overall extent of injury as well as gross pathologic changes, two important characteristics used in the evaluation of therapeutic interventions. With continued technological improvements in in vivo MR imaging, this technique will continue to be an important analytical tool in the study of SCI.

In some regions, in vivo MR images, collected on a 4.7T magnet, appear different from in vitro MR images collected on a 14.1T magnet. The in vivo MR images were collected by using T2-weighted fast spin-echo sequences, whereas in vitro MR images were collected by using proton attenuation–weighted spin-echo sequences. In vivo MR images show cavitation as hyperintense signals due to T2-weighting, which is comparable to what is used in human MR imagings. This is in contrast with in vitro MR images, because cavities appear isointense due to proton attenuation weighting.

A limited number of studies have used in vivo MR imaging in experimental animal models, with an even smaller number by using in vitro MR imaging techniques. In the present study, we have used customized hardware (coils) and high magnetic fields to obtain high-quality in vivo and in vitro images in the rat. Continued improvement of these MR components should lead to an increased utility of these methods. In our study, in vivo MR images show high resolution and greater pathologic detail than reported in previous MR imaging studies at this magnetic field

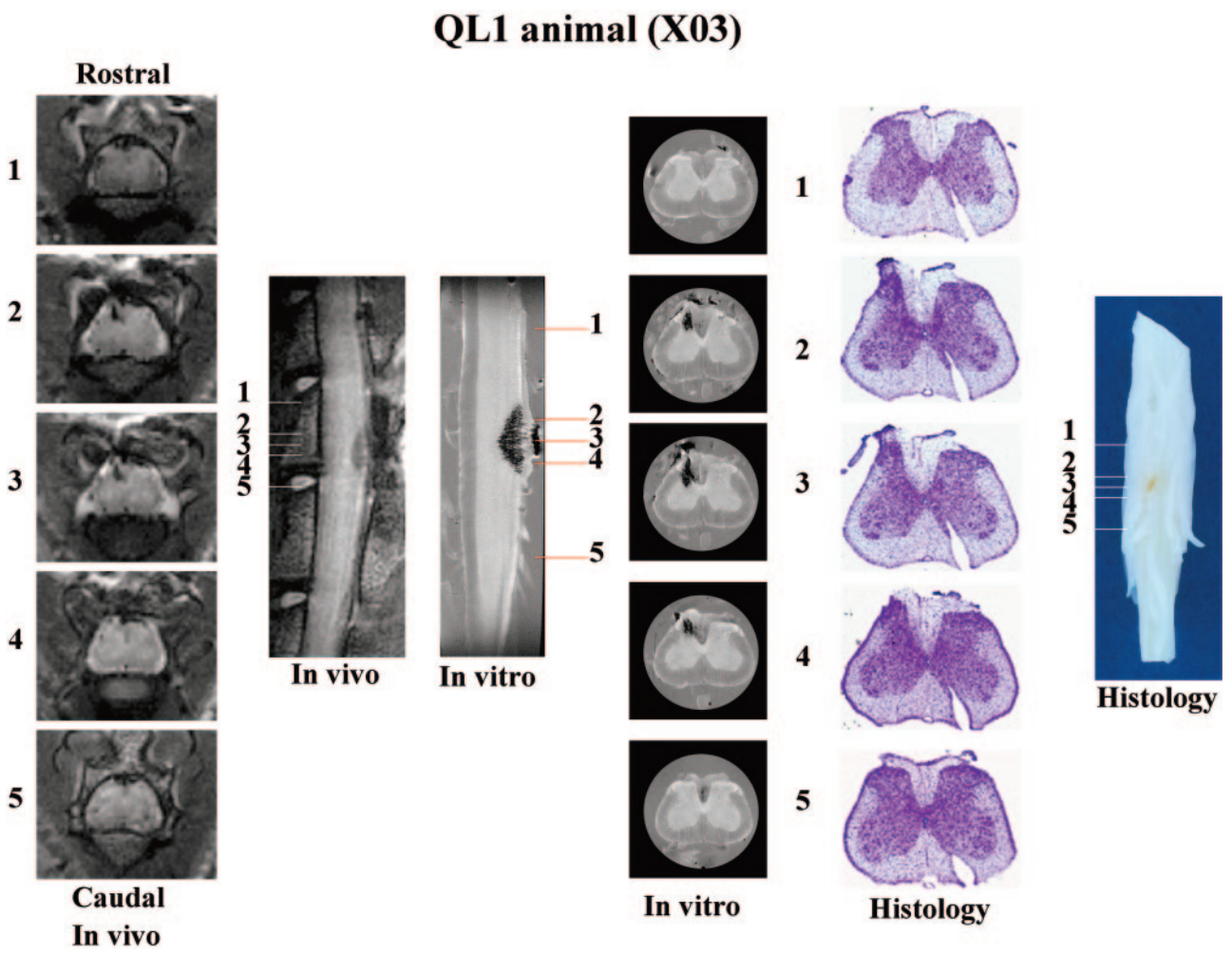

FIG 6. Summary of in vivo, in vitro, and histologic data collected for a representative QL1 animal (X03). Representative sections (1–5) are sampled with each method from the same rostrocaudal location in the spinal cord. Image sizes are the same as in Figs 2 and 3. See Fig 1, for labeling of anatomic and pathologic findings. Although sagittal images show the rostral-caudal extent of the injury, transverse sections provide greater detail of the pathologic changes associated with this injury model.

strength or lower (5, 15, 41–44). As expected, higher-quality MR images can be obtained at higher magnetic fields (36, 45) or with chronically implanted MR coils (6, 16, 46–50). Although we have been involved in the development of implanted coil technology (46, 50), we did not use implanted coils in this study because we wanted to eliminate the possible confounding effects of coil implantation and risk additional damage to the cord. By comparing the results of in vitro and histologic methods, details seen in vivo can be confirmed, thus strengthening the rationale for by using in vivo MR imaging as an important tool in the study of SCI.

Conclusions

High-resolution MR imaging can be used to study experimental SCI quantitatively and qualitatively with high field magnets by using customized coils and optimized methods. In the present study in vivo MR imaging was sensitive enough to detect significant differences in pathologic characteristics between two different strategies of injury (QL1 vs QL2). Although significant differences were found among injury lengths calculated from in vivo and in vitro images, they were within the range of difference in the section thickness for each method used. These results indicate that in vivo MR imaging may underestimate total injury length by no more than one section thickness due to volume averaging in the end sections. This suggests that in vivo MR imaging methods have the potential to be used in longitudinal studies in the same animal to evaluate the progression of pathologic changes as well as the efficacy of therapeutic interventions to repair and protect the injured spinal cord. Studies are presently underway to evaluate the effects of neuroprotective strategies on the progression of pathologic changes (ie, cavitation, hemorrhage, and edema) and BSCB disruption following excitotoxic SCI. In the future, another approach that will be used, which has become an important tool to map the organization of white matter fibers in the injured spinal cord, is diffusion-weighted imaging (19, 51). The capability to map white matter fibers may allow

the determination of the effects of injury on selected ascending and descending pathways in the injured cord.

Acknowledgments

We thank Gary Blaskowski for his expert imaging assistance, Ty Black for providing his expertise with image processing, and Dr. Joseph Riley for his expert assistance with statistical analysis. All MR imaging data were obtained at the Advanced Magnetic Resonance Imaging and Spectroscopy facility in the McKnight Brain Institute at the University of Florida. The work was supported by the McKnight Brain Institute at the University of Florida Neurotrauma Research Seed Program and National Institutes of Health grants R01 NS40096 (to R.P.Y.), R01 NS42075 (to T.H.M.), and P41 RR16105 (to T.H.M.).

References

1. Yezierski RP. **Pathophysiology and animal models of spinal cord injury pain.** In: Yezierski RP, Burchiel K, eds. *Spinal cord injury pain: assessment, mechanisms, management.* Seattle: IASP Press;2002:117–136
2. Yezierski RP, Santana M, Park SH, Madsen PW. **Neuronal degeneration and spinal cavitation following intraspinal injections of quisqualic acid.** *J Neurotrauma* 1993;10:445–456
3. Yezierski RP, Liu S, Ruenes GL, et al. **Excitotoxic spinal cord injury: behavioral and morphological characteristics of a central pain model.** *Pain* 1998;75:141–155
4. Falconer JC, Narayana PA, Bhattacharjee MB, Liu SJ. **Quantitative MRI of spinal cord injury in a rat model.** *Magn Reson Med* 1994;32:484–491
5. Ohta K, Fujimura Y, Watanabe M, Yato Y. **Experimental study on MRI evaluation of the course of cervical spinal cord injury.** *Spinal Cord* 1999;37:580–584
6. Bilgen M, Abbe R, Liu SJ, Narayana PA. **Spatial and temporal evolution of hemorrhage in the hyperacute phase of experimental spinal cord injury: *in vivo* magnetic resonance imaging.** *Magn Reson Med* 2000;43:594–600
7. Flanders AE, Schaefer DM, et al. **Acute cervical spine trauma: correlation of MR imaging findings with degree of neurologic deficit.** *Radiology* 1990;177:25–33
8. Yamashita Y, Takahashi M, Matsuno Y. **Chronic injuries of the spinal cord: assessment with MR imaging.** *Radiology* 1990;175:849–854
9. Yamashita Y, Takahashi M, Matsuno Y. **Acute spinal cord injury: magnetic resonance imaging correlated with myelopathy.** *Br J Rad* 1991;64:201–209
10. Ohshio I, Hatayama A, Kaneda K, et al. **Correlation between histopathologic features and magnetic resonance images of spinal cord lesions.** *Spine* 1993;18:1140–1149
11. Flanders AE, Spettell CM, Friedman DP, et al. **The relationship between the functional abilities of patients with cervical spinal cord injury and the severity of damage revealed by MR imaging.** *AJNR Am J Neuroradiol* 1999;20:926–934
12. Selden NR, Quint DJ, Patel N, et al. **Emergency magnetic resonance imaging of cervical spinal cord injuries: clinical correlation and prognosis.** *Neurosurgery* 1999;44:785–792
13. Rattliff J, Voorhies R. **Increased MRI signal intensity in association with myelopathy and cervical instability: case report and review of the literature.** *Surg Neurol* 2000;53:8–13
14. Ishida Y, Tominaga T. **Predictors of neurologic recovery in acute central cervical cord injury with upper extremity impairment.** *Spine* 2002;27:1652–1657
15. Runge VM, Wells JW, Baldwin SA, et al. **Evaluation of the temporal evolution of acute spinal cord injury.** *Invest Radiol* 1997;32:105–110
16. Bilgen M, Abbe R, Narayana PA. **Dynamic contrast-enhanced MRI of experimental spinal cord injury: *in vivo* serial studies.** *Magn Reson Med* 2001;45:614–622
17. Bilgen M, Narayana PA. **A pharmacokinetic model for quantitative evaluation of spinal cord injury with dynamic contrast-enhanced magnetic resonance imaging.** *Magn Reson Med* 2001;46:1099–1106
18. Bilgen M, Dogan B, Narayana PA. ***In vivo* assessment of blood-spinal cord barrier permeability: serial dynamic contrast enhanced MRI of spinal cord injury.** *Magn Reson Imaging* 2002;20:337–341
19. Guilfoyle DN, Helpern JA, Lim KO. **Diffusion tensor imaging in fixed brain tissue at 7.0 T.** *NMR Biomed* 2003;16:77–81
20. Yezierski RP. **Pain following spinal cord injury: pathophysiology and central mechanisms.** *Prog Brain Res* 2001;129:429–449
21. Gorman AL, Yu CG, Ruenes GR, et al. **Conditions affecting the onset, severity, and progression of a spontaneous pain-like behavior after excitotoxic spinal cord injury.** *J Pain* 2001;2:229–240
22. Yu CG, Fairbanks CA, Wilcox GL, Yezierski RP. **Effects of agmatine, interleukin-10, and cyclosporine on spontaneous pain behavior after excitotoxic spinal cord injury in rats.** *J Pain* 2003;4:129–140
23. Haase A, Frahm J, Hanicke W, Matthaei D. **1H NMR chemical shift selective (CHESS) imaging.** *Phys Med Biol* 1985;30:341–344
24. Bancroft JD, Cook HC. **Pigments.** In: *Manual of histological techniques.* Edinburgh: Churchill Livingstone;1984:151–152
25. Plunkett JA, Yu CG, Easton J, et al. **Effects of interleukin-10 (IL-10) on pain behavior and gene expression following excitotoxic spinal cord injury in the rat.** *Exp Neurol* 2001;168:144–154
26. Schwartz ED, Falcone SF, Quencer RM, Green BA. **Posttraumatic syringomyelia: pathogenesis, imaging, and treatment.** *AJNR Am J Neuroradiol* 1999b;173:487–492
27. Madsen PW, Yezierski RP, Holets VR. **Syringomyelia: clinical observations and experimental studies.** *J Neurotrauma* 1994;11:241–254
28. Williams B. **Post-traumatic syringomyelia, an update.** *Paraplegia* 1990;28:296–313
29. Oakes WJ. **Chiari malformations, hydromyelia, syringomyelia.** In: Wilkins RH, Rengachary SS, eds. *Neurosurgery.* New York: McGraw-Hill;1996:3593–3616
30. Wirth ED III, Vierck CJ, Reier PJ, et al. **Correlation of MRI findings with spinal cord injury pain following neural tissue grafting into patients with post-traumatic syringomyelia.** In: Yezierski RP, Burchiel KJ, eds. *Spinal cord injury pain: assessment, mechanisms, management.* Seattle: IASP Press;2002:313–330
31. Weirich SD, Cotler HB, Narayana PA, et al. **Histopathologic correlation of magnetic resonance imaging signal patterns in a spinal cord injury model.** *Spine* 1990;15:630–638
32. Wirth ED III, Theele DP, Mareci TH, et al. **In vivo magnetic resonance imaging of fetal cat neural tissue transplants in the adult cat spinal cord.** *J Neurosurg* 1992;76:261–274
33. Wirth ED III, Theele DP, Mareci TH, et al. **Dynamic assessment of intraspinal neural graft survival using magnetic resonance imaging.** *Exp Neurol* 1995;136:64–72
34. Schwartz ED, Yezierski RP, Pattany PM, et al. **Diffusion-weighted MR imaging in a rat model of syringomyelia after excitotoxic spinal cord injury.** *AJNR Am J Neuroradiol* 1999;20:1422–1428
35. Metz GA, Curt A, van de Meent H, et al. **Validation of the weight-drop contusion model in rats: a comparative study of human spinal cord injury.** *J Neurotrauma* 2000;17:1–17
36. Bonny JM, Gaviria M, Donnat JP, et al. **Nuclear magnetic resonance microimaging of mouse spinal cord in vivo.** *Neurobiol Dis* 2004;15:474–482
37. Yezierski RP, Culberson JL, Brown PB. **Cells of origin of propriospinal connections to cat lumbosacral gray as determined with horseradish peroxidase.** *Exp Neurol* 1980;69:493–512
38. Menetrey D, de Pommery J, Roudier F. **Propriospinal fibers reaching the lumbar enlargement in the rat.** *Neurosci Lett* 1985;31:257–261
39. Rapoport SI. **Pathological alterations of the blood brain barrier.** In: *Blood-brain barrier in physiology and medicine*. New York: Raven Press;1976:129–152
40. Bradbury M. **Breakdown of the blood-brain barrier.** In: *The concept of a blood-brain barrier.* Chichester, UK: Wiley;1979:351–382
41. Hackney DB, Asato R, Joseph PM, et al. **Hemorrhage and edema in acute spinal cord compression: demonstration by MR imaging.** *Radiology* 1986;161:387–390
42. Fraidakis M, Klason T, Cheng H, et al. **High-resolution MRI of intact and transected rat spinal cord.** *Exp Neurol* 1998;153:299–312
43. Iannotti C, Li H, Stemmler M, et al. **Identification of regenerative tissue cables using *in vivo* MRI after spinal cord hemisection and schwann cell bridging transplantation.** *J Neurotrauma* 2002;19:1543–1554
44. Brodbelt AR, Stoodley MA, Watling A, et al. **The role of exci-**

totoxic injury in post-traumatic syringomyelia. *J Neurotrauma* 2003;20:883–893
45. Franconi F, Lemaire L, Marescaux L, et al. ***In vivo*** **quantitative microimaging of rat spinal cord at 7T.** *Magn Reson Med* 2000;44:893–898
46. Wirth ED III, Mareci TH, Beck BL, et al. **A comparison of an inductively coupled implanted coil with optimized surface coils for *in vivo* NMR imaging of the spinal cord.** *Magn Reson Med* 1993;30:626–633
47. Ford JC, Hackney DB, Joseph PM, et al. **A method for *in vivo* high resolution MRI of rat spinal cord injury.** *Magn Reson Med* 1994;31:218–223
48. Fenyes DA, Narayana PA. ***In vivo*** **echo-planar imaging of rat spinal cord.** *Magn Reson Imaging* 1998;16:1249–1255
49. Narayana P, Abbe R, Liu S, Johnston D. **Does loss of gray- and white-matter contrast in injured spinal cord signify secondary injury? *In vivo* longitudinal studies.** *Magn Reson Med* 1999;41:315–320
50. Silver X, Ni X, Mercer EV, et al. ***In vivo*** **1H magnetic resonance imaging and spectroscopy of the rat spinal cord using and inductively-coupled chronically implanted RF coil.** *Magn Reson Med* 2001;46:1216–1222
51. Beaulieu C. **The basis of anisotropic water diffusion in the nervous system: a technical review.** *NMR Biomed* 2002;15:435–455